ACS Partner Journal

Journal of the American Society for Mass Spectrometry

pubs.acs.org/jasms

Article

Native Mass Spectrometry Dissects the Structural Dynamics of an Allosteric Heterodimer of SARS-CoV-2 Nonstructural Proteins

Stephanie M. Thibert,[†] Deseree J. Reid,[†] Jesse W. Wilson,[†] Rohith Varikoti, Natalia Maltseva, Katherine J. Schultz, Agustin Kruel, Gyorgy Babnigg, Andrzej Joachimiak, Neeraj Kumar, and Mowei Zhou*

Cite This: *J. Am. Soc. Mass Spectrom.* 2024, 35, 912−921

Read Online

ACCESS | Metrics & More | Article Recommendations | Supporting Information

ABSTRACT: Structure-based drug design, which relies on precise understanding of the target protein and its interaction with the drug candidate, is dramatically expedited by advances in computational methods for candidate prediction. Yet, the accuracy needs to be improved with more structural data from high throughput experiments, which are challenging to generate, especially for dynamic and weak associations. Herein, we applied native mass spectrometry (native MS) to rapidly characterize ligand binding of an allosteric heterodimeric complex of SARS-CoV-2 nonstructural proteins (nsp) nsp10 and nsp16 (nsp10/16), a complex essential for virus survival in the host and thus a desirable drug target. Native MS showed that the dimer is in equilibrium with monomeric states in solution. Consistent with the literature, well characterized small cosubstrate, RNA substrate, and product bind with high specificity and affinity to the dimer but not the free monomers. Unsuccessfully designed ligands bind indiscriminately to all forms. Using neutral gas collision, the nsp16 monomer with bound cosubstrate can be released from the holo dimer complex, confirming the binding to nsp16 as revealed by the crystal structure. However, we observed an unusual migration of the endogenous zinc ions bound to nsp10 to nsp16 after collisional dissociation. The metal migration can be suppressed by using surface collision with reduced precursor charge states, which presumably resulted in minimal gas-phase structural rearrangement and highlighted the importance of complementary techniques. With minimal sample input (∼μg), native MS can rapidly detect ligand binding affinities and locations in dynamic multisubunit protein complexes, demonstrating the potential of an "all-in-one" native MS assay for rapid structural profiling of protein-to-AI-based compound systems to expedite drug discovery.

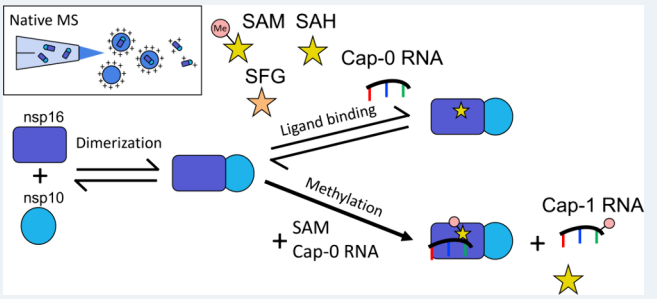

INTRODUCTION

Structure-based drug design (SBDD) is one approach for accelerated discovery of new compounds[1] with therapeutic potential that focuses on finding small molecule inhibitors that bind to target proteins' active sites. The recent progress in artificial intelligence (AI) and machine learning (ML) has greatly elevated the efficiency of *in silico* screening for potential compounds, offering considerable savings in time and resources compared to traditional experimental screening methods. However, this approach can be prone to errors if not executed thoughtfully.[2] While AI/ML both benefit from training with large data sets, current high-throughput experimental screening methods only provide activity and phenotypical data.[3−5] Structural details that can be quantitatively interfaced with first-principle calculations such as docking and molecular dynamics (MD) simulations are often lacking. Therefore, classical structural biology methods remain the primary source of high-quality structural data, but they are resource- and labor-intensive and are usually applied only at a later stage of the screening on a limited number of protein−ligand complexes.

Native mass spectrometry (native MS) characterizes noncovalent complexes under nondenaturing conditions and can provide fast assessment (typically in minutes) of protein−protein and protein−ligand interactions using small quantities (∼μg) of often precious samples.[6−9] Although native MS requires specialized methods distinct from common MS applications, recent advances in commercial instrumentation and automated systems have significantly increased the accessibility of the technology.[10−14] The methodologies for studying protein−ligand interactions have been reviewed in detail recently.[15] However, most applications focus on the

Received: December 27, 2023
Revised: February 2, 2024
Accepted: February 7, 2024
Published: March 27, 2024

intact mass measurement at the MS1 level. Tandem MS with a variety of fragmentation techniques can reveal more information from the primary sequence to higher order structure.[16] For multimeric protein complexes in particular, ligand binding locations can be assessed by gas-phase dissection of the protein−ligand complex.[15] Collision-based activation methods are often effective in breaking noncovalent interactions to probe which subunit holds the ligand binding site. Electron- and photon-based activation methods can yield protein backbone fragments and inform the binding site at the amino acid level, although most reported cases so far are on monomeric proteins. A few reports have thoroughly investigated the dissociation of ligands from protein complexes using collision-induced dissociation (CID, gas collision) or surface-induced dissociation (SID).[17−22] While the gas-phase experiments generally reflect known structural biology data and can inform structural details, the extent to which ligands are retained on released subunits after activating the complex differ for each case. Parameters in the ion source and tandem MS methods determine the internal energy deposition and undoubtedly affect the ligand retention.[22] In addition, structures and charge states of the protein−ligand complexes appear to also play a role.[17,19] For example, Klassen et al.[19] observed a minor CID pathway of ligand migration for cholera toxin B subunit homopentamer and streptavidin homotetramer, which was attributed to a structural change unique to the gas phase. The conflicting data in the literature indicates gas-phase activation may induce structural alterations that are protein or ligand specific and may not be "linearly" correlated with solution-phase structures. Therefore, further studies and more data are needed to improve our understanding about the underlying mechanisms of different protein−ligand systems for better interpretation of native MS data. This can be extremely useful for characterizing unknown and dynamic structures that are not well-defined by conventional structural biology techniques, where no easy reference data sets are available for validation.

Herein, we studied the native MS behavior of an allosteric complex of the two nonstructural proteins (nsp) nsp10 and nsp16 heterodimer from SARS-CoV-2. The nsp10/16 heterodimer is part of the SARS-CoV-2 RNA replication and transcription complex.[23] Nsp10/16 heterodimer is an enzyme-2′-O methyltransferase with nsp16 serving as a catalytic unit and nsp10 functioning as an allosteric activator essential for enzyme activity. The complex methylates the ribose 2′-O of the first adenosine ribonucleotide of the nascent mRNA Cap-0-RNA to form Cap-1-RNA (m7GpppAm2′-O-RNA) using SAM (S-adenosyl-L-methionine) as the methyl donor and helps evade the host's immune response.[24−28] Nsp10 is essential to activate the methyltransferase (MTase) of nsp16[28] via an allosteric effect.[29−31] Inhibition of the methyltransferase activity may reduce viral proliferation, making the complex an attractive pan-coronavirus drug target considering its essential function and conservation in coronaviruses.[32] Unfortunately, limited success has been reported so far due to promiscuity and/or high cell toxicity, which are common failures also seen for other nsp targets.[4,33,34] Although the accumulated data inform future developments, the dynamic nature of such protein structures may have been underappreciated in SBDD. A recent computational study reported a cryptic pocket in nsp10/16 as a new target,[29] which was recently validated by experiments and led to alternative design strategies.[34] These advances highlight the need for more versatile tools to characterize dynamic protein assemblies for SBDD.

Our native MS measurements showed generally similar binding strength as published values but provided more details on the heterogeneity of the system, including a dynamic monomer−dimer equilibrium in solution that was implied in previous reports but may have been overlooked in solved crystal structures. Native MS also detected the specific binding of substrates to the allosteric heterodimer complex and allowed differentiation of nonspecific binding of designed compounds. Dissecting the heterodimer in the gas phase further revealed the binding location of the substrates. We also observed an unusual metal migration behavior in CID and SID, which can be minimized in SID at reduced charge state. This was likely a gas-phase effect but also relevant to the dynamics of the protein structure worth further investigation. The unique information and the fast speed of native MS has great potential to rapidly supply molecular mechanisms for applications such as AI-based drug design.

EXPERIMENTAL SECTION

Protein Expression and Purification. The *nsp10* and *nsp16* genes were synthesized (Twist Bioscience) and cloned into the pMCSG53 vector. Proteins were expressed and purified as reported previously[35] with small differences in buffer compositions described below. Additionally, the His tag was successfully cleaved from the proteins with TEV protease following a previously described protocol.[36] Protein amino acid sequences are listed in Table S1.

Harvested cells were resuspended in 5 volumes of buffer (50 mM HEPES pH 8.0, 500 mM NaCl, 20 mM imidazole, 5% v/v glycerol, 1 μM $MgCl_2$, 1 μM $ZnCl_2$, and 10 mM 2-mercaptoethanol, Sigma) and then sonicated and centrifuged to obtain the soluble fraction for protein purification.

Proteins were purified using Ni^{2+}-immobilized metal affinity chromatography (IMAC) with 3 mL of Ni^{2+} Sepharose (GE Healthcare Life Sciences) equilibrated with lysis buffer (HEPES pH 8.0, 500 mM NaCl, 30 mM imidazole, 5% v/v glycerol, 1 mM $MgCl_2$, and 1 mM TCEP (tris(2carboxyethyl)-phosphine, Amresco, Inc.)) in a Flex-Column (420400-2510) connected to a Vac-Man vacuum manifold (Promega). Nsp10 and Nsp16 proteins were eluted with lysis buffer that was supplemented with 500 mM imidazole. The proteins were exchanged into imidazole-free buffer (50 mM HEPES pH 8.0, 500 mM NaCl, 5% v/v glycerol, 1 mM MgCl2, and 1 mM TCEP) and TEV was added for overnight cleavage with a 1:250 ratio of protease to protein for Nsp10 and a 1:150 ratio of protease to Nsp16 protein.

Cleaved proteins were purified using a second step of IMAC (IMAC-II) with a HiTrap Chelating HP column charged with Ni^{2+} on an AKTA Express System (GE Healthcare) followed by size-exclusion chromatography with a Superdex 200 Increase 10/300 GL column equilibrated with storage buffer (10 mM HEPES pH 7.5, 150 mM NaCl, 5% glycerol and 1 mM TCEP). The purest fractions of Nsp10 and Nsp16 proteins were mixed in a 1:1 ratio in HEPES buffer pH 7.4 to a final concentration of the complex at 2.4 mg/mL.

Native Mass Spectrometry (Native MS). Before native MS, the proteins were buffer exchanged into 100 mM ammonium acetate solutions, protein concentrations remeasured using nanodrop, and then supplemented with expected ligands (SAM, SAH, Cap-0 RNA, SFG). SAM, SAH (S-adenosyl-L-homocysteine), and SFG (sinefungin) were all

https://doi.org/10.1021/jasms.3c00453
J. Am. Soc. Mass Spectrom. 2024, 35, 912−921

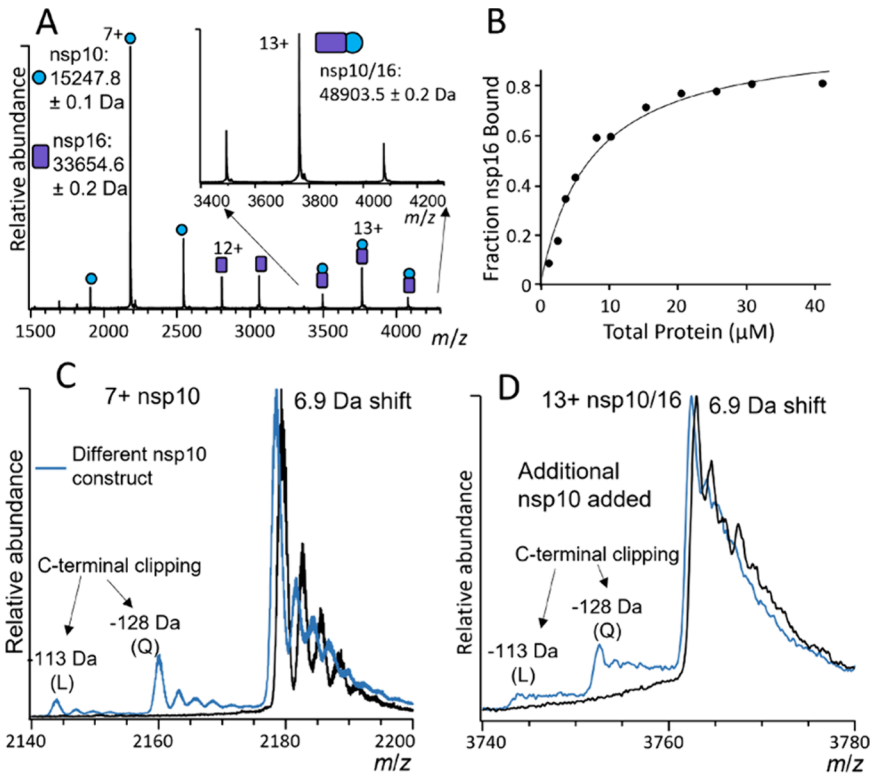

Figure 1. (A) Native MS spectrum showing 10 μM of a mixture of nsp10, nsp16, and the heterodimer. The inset shows the magnified display of the dimer peaks. (B) Dimer formation can be directly tracked by the changing intensities as a function of protein concentration. (C) A different construct of nsp10' (blue trace) has 6.9 Da lower mass and extra terminal clipping peaks from the original nsp10 (black trace). (D) Mixing ~33 μM of the nsp10' with 10 μM of the original nsp10/16 resulted in subunit exchange in the dimer, as manifested by the mass shift in the dimer peak (black to blue trace).

purchased from Sigma with catalog numbers A7007, A9384, and S8559, respectively. Cap-0 RNA (m^7GpppAUUAAA) was purchased from Bio-Synthesis, Inc. (Lewisville, TX, USA). Native MS experiments were performed to observe the formation of the nsp10/16 heterodimer and to track ligand binding on a Synapt G2si quadrupole ion mobility time-of-flight mass spectrometer (Waters, Manchester, UK). Static nanoelectrospray was used to infuse the protein solution at ~0.7 kV voltage and 30 °C, using in-house pulled borosilicate glass capillaries (ID 0.78 mm, item no. BF100-78-10, Sutter Instruments, Novato, CA, USA) using a Sutter Instrument pipet puller P-1000 (Novato, CA, USA). Cone voltage was 100 V. Ion mobility was enabled, with traveling wave in the mobility cell set to 400 m/s and 20 V. For MS/MS experiments, the individual charge state was isolated by the quadrupole. Direct dissociation of isolated protein complexes was either by CID using trap collision energy (Trap CE) or SID via custom modification.[37] The SID collision energy was controlled also via the trap collision energy and the collector/stopper voltage in the System voltage tab as described in the recent publication.[37]

Native MS Data Analysis. Data analysis was performed using UniDec deconvolution software.[38] For nsp10/16 dimerization and ligand binding, the m/z spectra were deconvolved and nsp10, nsp16, nsp10/16, and ligand-bound peaks for all species were identified. Deconvolved peak areas were used for all binding analyses. To estimate the binding affinity for nsp10/16 dimerization, the fraction of nsp16 bound to nsp10 was calculated by dividing the dimer peak area by the sum of the peak areas of nsp16 monomer and dimer and plotted against free concentrations of nsp10. The data were fit to the Hill equation (eq 1)

$$\text{Fraction nsp16 bound} = y = \frac{B_{\max} \cdot \text{nsp10}^h}{K_d^h + \text{nsp10}^h} \quad (1)$$

where B_{max} is the maximum specific binding, nsp10 is the free concentration of nsp10, h is the hill coefficient, and K_d is the dissociation constant for nsp10/16 dimerization.

For ligand-binding studies, the ratio of ligand bound was calculated from the deconvolved peak areas as the quotient of the holo peak (ligand bound) area divided by the sum of the apo (ligand lost) and holo peak areas. Ligand binding data were fit to the single-site binding model, which is a simplified version of the Hill equation when h = 1, as shown in eq 2

$$\text{fraction ligand bound} = y = \frac{B_{\max} \cdot x}{K_d + x} \quad (2)$$

where x is the free concentration of SAM, SAH, or SFG.

All K_d estimates were completed by fitting the data to the specified binding model using the cftool function in Matlab. For the characterization of collision-induced dissociation of ligands from the nsp monomers and heterodimer, MetaUniDec[39] was used to extract the areas of the holo and apo peaks as a function of collision voltage. Raw, Unidec configuration files, and ligand K_d calculation files are available at MassIVE (https://massive.ucsd.edu/ Accession: MSV000092776).

Molecular Dynamics. For initial structures, we used the nsp10/16 complex predicted from docking simulations and performed all-atom molecular dynamics (MD) simulations

https://doi.org/10.1021/jasms.3c00453
J. Am. Soc. Mass Spectrom. 2024, 35, 912−921

using GROMACS v2018.6.[40] We adopted the Amber FF14SB force field[41] for the complex and the TIP3P water model[42] with Joung and Cheatham ion parameters[43] were used for water and neutralizing monovalent ions in the system. The initial system was minimized by the conjugated gradient algorithms up to a maximum residual force of 10.0 kJ/mol. Then, the system was equilibrated at 300 K for 500 ps under the NVT ensemble using the Berendsen velocity rescaling method followed by 1 ns with the NPT ensemble using the Berendsen pressure coupling method by constraining both the protein and ligand.[44] As a next step, we performed 50 ns production MD simulations with a 2 fs time step at 300 K and 1 atm using the Parrinello−Rahman pressure coupling method[45] without any restraints. The particle mesh Ewald algorithm[46] was used to evaluate long-range electrostatic interactions. Then, we analyzed and compared the root-mean-square deviation (RMSD) and root-mean-square fluctuation (RMSF) for the nsp16 and nsp10/16 dimer to determine the conformational changes and contribution of each amino acid to the motion of proteins, using the GROMACS rms and rmsf modules. We computed the hydrogen bonds and salt bridges formed between the interface residues using hbond and saltbr modules and their residue−residue correlation using covar and anaeig modules.

***In Silico* Compound Design.** We generated a library of candidate molecules based on molecular scaffolds obtained from a literature search of validated nsp10/16 inhibitors. Candidate compounds were screened based on molecular descriptors, physicochemical properties, toxicity estimates, and molecular docking simulations to filter out undesirable compounds as discussed in our previous work.[4,5] The details of our *in silico* compound generation and down-selection process will be discussed in a separate manuscript currently in preparation. The top candidate resulting from in silico ligand- and structure-based assessments was used for further experimental validation.

RESULTS AND DISCUSSION

Native MS and Subunit Exchange Suggest nsp10/16 Is a Dynamic Dimer in Equilibrium. We separately expressed and purified nsp10 and nsp16 from SARS-CoV-2 in *E. coli* cells and mixed them at equimolar ratios in HEPES buffer to form the heterodimer nsp10/16 as previously described.[24] The proteins were then buffer exchanged into 100 mM ammonium acetate (AA) solution for native MS. The native MS spectrum (Figure 1A) showed a mixed population of nsp10 monomer, nsp16 monomer, and nsp10/16 heterodimer. The mass of nsp10 was 127.9 Da larger than the mass measured under the denaturing state (Figure S1) due to presence of two zinc ions (Zn^{2+}) that are known to be essential for nsp10 function.[26,47,48] The relative abundance of the dimer increased with higher protein concentration (Figure 1B), allowing us to plot a binding curve based on the native MS data and estimate a K_d of 1.4 μM (Figure S2A). Despite the different signal response (e.g., ionization efficiency) between nsp10 and nsp16 that could complicate the analysis (Figure S2B),[49] our estimation is similar to the apparent K_d of MERS nsp10/16 (2 μM) reported by activity assay.[30] Methods to account for differences in signal response during binding affinity studies[50] by native MS, such as slow mixing mode (SLOMO),[50] could be implemented in future studies.

The free monomers detected in native MS prompted further investigation into the dynamic nature of the dimer assembly.

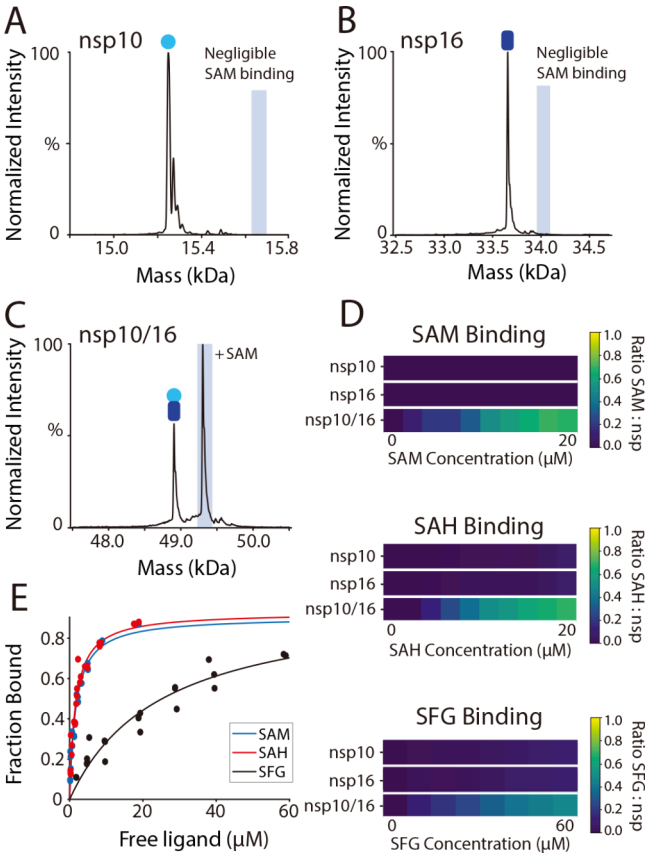

Figure 2. Deconvolved mass spectra for 6 μM SAM binding to (A) nsp10, (B) nsp16, and (C) nsp10/16 complex. The heat maps (D) show the percentage of the total peak area that is ligand-bound for each species as the ligand concentration was increased from 0−20 μM for SAM and SAH and from 0−60 μM for SFG. Estimated K_d curves (E) are shown for each ligand when fit to a single-site binding model.

First, our molecular dynamics (MD) simulations of the heterodimer crystal structure in water solvent corroborated the reported allosteric effect of nsp10 binding to nsp16 (Figure S3) and also revealed many transient interfacial hydrogen bonds and salt bridges (Figure S4). Second, we mixed the heterodimer with another nsp10 construct with a −6.9 Da mass shift from different purification tag sequences (Figure 1C, sequence difference in Table S1). The mixing in solution prior to MS resulted in the appearance of a −6.8 ± 0.3 Da mass shift on nsp10/16 in the native MS spectrum (Figure 1D). The nsp10' was added in about 3-fold molar excess, therefore making the nsp10' the dominant species in the spectra. The transient interfacial interactions in MD and the exchange of subunits in solution suggested a dynamic equilibrium between the monomeric and dimeric states. Interestingly, the crystal structure of nsp16 monomer has not been reported. Isolated nsp10 was recently resolved structurally, which showed minimal rearrangement compared to its form in the heterodimer structure, complementing our MD results. Equilibrium between monomer and homodimer states of nsp10 was also noted.[51] Taken together, these results highlight that besides the known active form of nsp10/16, nsp10, and nsp16 are likely relevant and should not be ignored in SBDD.

Known Substrates Specifically Bind to the Dimeric State of nsp10/16 in Native MS. We then probed the binding specificity of several known ligands to nsp10, nsp16, and nsp10/16 by native MS. The S-adenosyl-L-methionine

https://doi.org/10.1021/jasms.3c00453
J. Am. Soc. Mass Spectrom. 2024, 35, 912−921

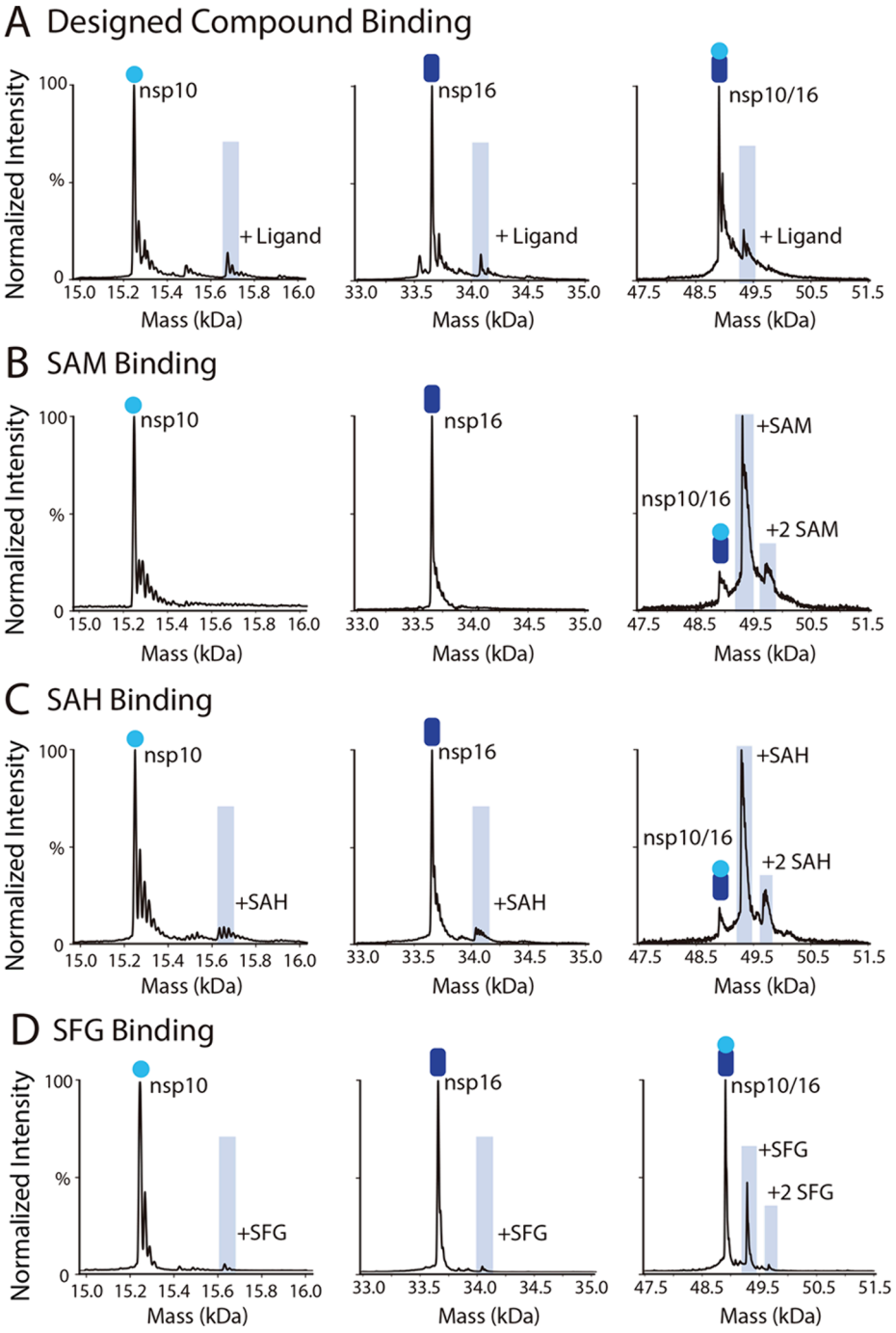

Figure 3. Deconvolved mass spectra of nsp10, nsp16, and nsp10/16 at 20 μM added ligand. (A) Binding of the designed compound was nonspecific, indiscriminately binding to the dimer and monomers. (B) In contrast, SAM displayed negligible binding to monomers but specific and significant binding to the dimer, with a lower but distinct second SAM binding event clearly visible. Like SAM, SAH (C) and SFG (D) also predominantly bind to the dimer and display a second peak corresponding to two bound ligands. However, unlike SAM, the small ligand peaks in the monomer spectra indicate that some degree of nonspecific binding occurs.

(SAM) cosubstrate binds to nsp16, stabilizes nsp10/16, and serves as the methyl donor for MTase activity during viral RNA capping. Cap-0 RNA substrate binds to the active site and is converted to the mature Cap-1 RNA by methyl transfer from the SAM, and generation of S-adenosyl-L-homocysteine (SAH) product.[24,27,31,48] A pan-MTase inhibitor sinefungin (SFG) occupies the SAM and SAH binding site in cocrystals with nsp10/16 and has been used as a model to inform inhibitor design.[26,27] We performed native MS with increasing concentrations of cosubstrate SAM, product SAH, and inhibitor SFG to 5 μM protein.

The relative abundances of the apo vs holo populations for nsp10, nsp16, and nsp10/16 were plotted in Figure 2. All compounds bound primarily to nsp10/16, consistent with the isothermal titration calorimetry (ITC) binding assays using individual proteins.[28] The proteins' ionization efficiencies did not change significantly within these ligand concentrations (Figure S5). Therefore, we used a single-site binding model to calculate the apparent binding affinities of the ligands for

https://doi.org/10.1021/jasms.3c00453
J. Am. Soc. Mass Spectrom. 2024, 35, 912−921

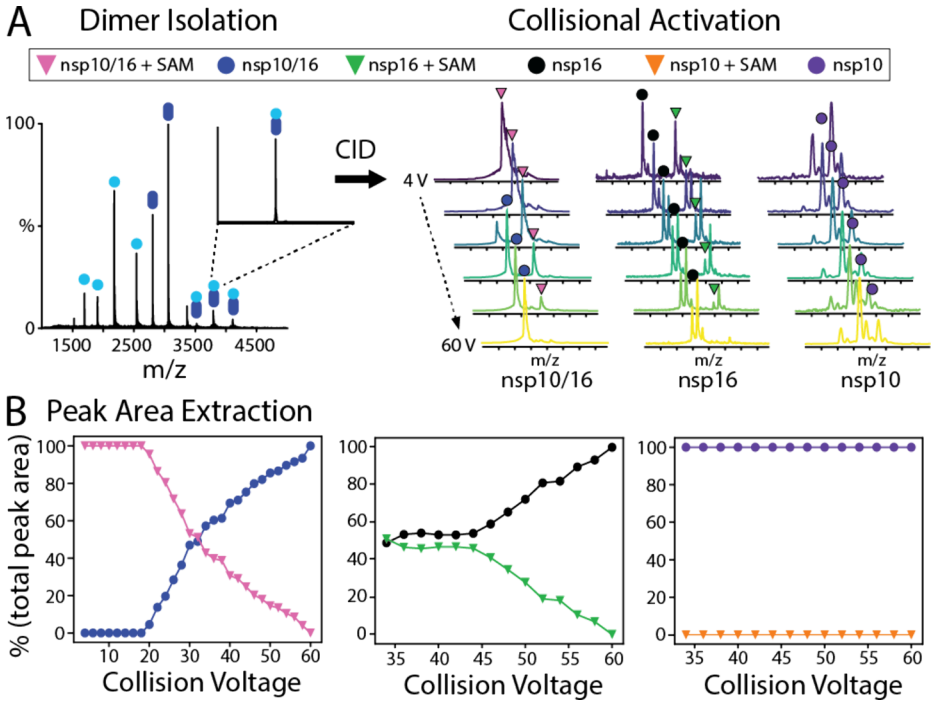

Figure 4. (A) Nsp10/16 was isolated from monomers and subjected to collisional dissociation in 2 V increments from 4 to 60 V. (B) Peak areas were extracted as a function of collision voltage and plotted for SAM-bound nsp10/16 (pink triangles), apo nsp10/16 (blue circles), SAM-bound nsp16 (green triangles), apo nsp16 (black circles), SAM-bound nsp10 (orange triangles), and apo nsp10 (purple circles). Additional peaks visible in the nsp10 and nsp16 spectra (A) are due to either 1 or 2 bound Zn ions.

nsp10/16. Binding affinities to SAM and SAH were similar to K_d of ~2 μM, while SFG showed much weaker binding at ~25 μM (Figure 2E and Figure S6), similar to the values reported previously using ITC.[52] At high ligand concentrations, we observed more than one compound binding per nsp10/16 heterodimer for all compounds, with calculated K_d values at least an order of magnitude higher than the first binding event and were not discussed here due to the likelihood of nonspecific binding.

Next, we tested a potential inhibitor designed computationally through our high throughput virtual screening (HTVS)[4,5] and ordered it from a drug library MCULE database (Mcule-ID: MCULE-8583086513-0). The specificity of binding was quickly assessed from native MS data with weak binding of the compound to not only nsp10/16 but also the monomers observed (Figure 3A). In contrast, binding of SAM/SAH/SFG displayed significant binding to nsp10/16 and only negligible binding to the monomers (Figure 3B–D). The relatively low affinity and promiscuity of this compound prevented us from pursuing detailed structural biology experiments in this study. Future developments utilizing native top-down methods could help reveal ligand binding regions for such weak interactions. The recent MD study proposed that the SAM binding pocket was in a more open state in the heterodimer than in the nsp16 monomer, and thus, any compound that binds indiscriminately to monomer and dimer forms is unlikely to follow the same binding mode as SAM,[29] possibly outside the predicted pocket. Echoing this prediction, an experimental study discovered a covalent inhibitor acting on the cysteine residues in a cryptic pocket near the active site preventing SAM binding.[34] Even in the crystal structures, multiple binding poses were proposed presumably due to the heterogeneity of the interactions. This may be at least partly attributed to the dynamics of proteins, which is not often considered in high throughput biochemical assays. Native MS can thus serve as a complementary approach to quickly assess such properties.

Bound Ligands in nsp10/16 Are Retained in the Released Monomers after Low Energy Collisions. "Complex-down"[53] can inform binding location of ligands in multimeric protein complexes, via the release of ligand bound subunits after gas-phase "heating" of the intact complex.[6] We m/z-isolated the SAM-bound holo dimer away from the monomeric states and dissociated the dimer in the mass spectrometer via gas collision (collision induced dissociation, CID). SAM was readily released in the low m/z region (Figure 4). The released nsp16 partially retained SAM, and high collision energy led to complete loss of substrates from the protein. Similar behavior was seen for SFG inhibitor (Figure S7). Interestingly, the nsp10/16-SFG complex appears to be more stable than the nsp10/16-SAM complex in CID, despite the lower K_d for SAM in solution. The CID collision voltage for 50% dissociation of ligand was ~48 V for SFG (Figure S7C) and ~30 V for SAM (Figure 4B). This gas-phase stability may originate from a different interaction with proteins for SAM and SFG. Alternatively, SAM binding may be destabilized more significantly upon CID due to altered structure or interaction with the allosteric regulator nsp10. Further investigation into the mechanism could help better correlate the gas-phase measurements with solution structures, especially in such dynamic systems that are challenging to study.

In contrast, cap-0 RNA bound strongly to nsp10/16 and nsp16 (Figure S8). The RNA bound to heterodimer also showed complete preservation of bound RNA in the released nsp16, regardless of collision energy (Figure S9), likely due to the enhanced electrostatic interactions between RNA and nsp16 in the gas phase. The detection of SAM and cap-0 RNA in the released nsp16 was consistent with the binding pockets within nsp16 observed in the crystal structures, suggesting that

https://doi.org/10.1021/jasms.3c00453
J. Am. Soc. Mass Spectrom. 2024, 35, 912−921

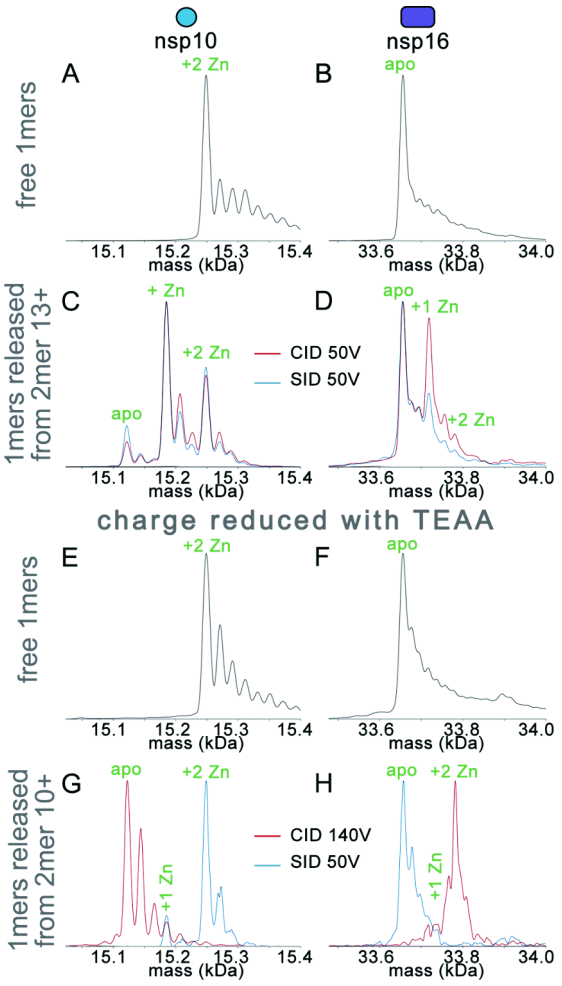

Figure 5. Deconvolved intact mass spectra of nsp10 (left column) and nsp16 (right column) monomers either as (A–B) free monomers in solution or (C–D) released from the heterodimer after dissociation. Data from CID are in red traces, and SID are in blue traces. Zn-bound stoichiometry is annotated above the peaks. Charge reduced condition with TEAA addition are in (E–H) following the same format. For the nsp10/16 dimer at 13+, both SID and CID resulted in similar levels of Zn transfer. TEAA did not affect the bound Zn on free nsp16 in solution prior to dissociation, but the Zn transfer was largely eliminated in SID after charge reduction while CID tends to induce a higher degree of Zn transfer.

such dissociation experiments can be used to probe which subunit the ligand binds to under optimized conditions. This crucial information can serve as feedback for affirming that the AI-designed compounds are targeting the appropriate component of a heterocomplex without having to solve the high-resolution structure. Additionally, we monitored enzyme activity, and inhibition in the presence of SFG inhibitor, by directly measuring formation of cap-1 RNA over time (Figure S10). Complementary SAM-to-SAH conversion was also measured in the same native MS experiment, highlighting the potential of native MS to simultaneously quantify multiple species relating to reaction kinetics within a single experiment using low sample quantities.

Unusual Metal Transfer Behavior between nsp10/16 Subunits Is Charge-State Dependent. Although cosubstrate binding was successfully probed by CID, we noticed an unusual transfer of Zn^{2+} on dissociated nsp10 and nsp16. The free monomers in native MS only showed two Zn^{2+} binding on nsp10 (Figure 5A,B), consistent with the crystal structure where Zn^{2+} binds in two discrete cysteine-rich motifs in nsp10. In contrast, each monomer released from the heterodimer in CID showed several new species corresponding to 0–2 Zn^{2+} binding (Figure 5C,D, red traces). One of the zinc ions is at the interface with nsp16, raising the possibility that some structural dynamics could result in metal transfer. The alternative explanation is that the metal transfer was primarily a gas-phase structural rearrangement. The metal transfer is reminiscent of the ligand migration previously observed in CID of ligated cholera toxin B homopentamer and streptavidin homotetramer[19] and is possibly related to the gas-phase structure and charge configuration unique to nsp10/nsp16. To further investigate this phenomenon, we also used an alternative activation method, surface-induced dissociation (SID), which is believed to induce faster heating of complexes with less unfolding and structural rearrangement than CID.[54,55] SID showed similar spectra as CID with significant zinc transfer (Figure 5C,D, blue traces) for the 13+ dimer.

We then resorted to charge reduction, which previously was shown to suppress gas-phase unfolding of protein complexes.[56,57] Using the solution additive triethylammonium acetate (TEAA) at 20 mM, the charge-state envelope of nsp10/16 shifted from 13+ down to 10+. TEAA itself did not affect the bound Zn^{2+} on the free nsp16 monomers in solution prior to dissociation (Figure 5E,F), but the zinc transfer was largely eliminated in SID (Figure 5G,H, blue traces). In contrast, CID required higher voltage to dissociate the heterodimer (>100 V) and instead near complete transfer of two zinc from nsp10 to nsp16 (Figure 5G,H, red traces). The reduced charge state presumably resulted in fewer charge configurations, reshaping the activation barriers for structural rearrangement and dissociation. Similar to previous reports, reducing charge state generally suppresses unfolding for SID, yielding more native-like dissociation products for structural elucidation.[56–58] While further experiments and computational modeling are needed to understand this charge-state-dependent zinc transfer, the results demonstrated that the dissociation experiment must be optimized to minimize structural rearrangements for obtaining the most relevant ligand-binding information to native-like states. Nonetheless, we hypothesize that this metal transfer behavior is correlated to the dynamic structure of nsp10/16 dimer and may be informative for characterization of similar but unknown structures.

CONCLUSION

In summary, we demonstrated that native MS could measure many structural aspects of the allosteric heterodimeric enzyme nsp10/16. Coexisting populations of inactive monomeric states and the active dimeric state can be resolved, and their ligand-binding properties separately examined. Monitoring time-resolved changes in enzymatic reactions is also feasible because of nondenaturing measurement. The “all-in-one” native MS assay offers molecular structure details that can serve as rapid feedback to computer-aided drug design. The additional capability of isolating and dissecting selected species can yield more structural information. However, our data suggest that migration of bound metal ions can occur but can be minimized with SID at reduced charge states. While we think gas-phase factors—especially charge—were the primary contributors to the observed metal transfer of the desolvated protein complex, the inherent structural dynamics may have also played a role. Further fundamental studies of the role of

https://doi.org/10.1021/jasms.3c00453
J. Am. Soc. Mass Spectrom. 2024, 35, 912–921

charge in the dissociation[59−61] are necessary to better correlate the gas-phase measurements with structure features in solution. Nonetheless, with many ongoing technical developments in dissociation methods,[6] native MS is anticipated to generate even more intricate structural information at amino acid residue resolution (e.g., ligand binding site). Such data will augment existing high-throughput screening methods and foster the creation of a mechanistic knowledge database for AI/ML models that will lead to improved success rates and throughput for drug discovery.

■ ASSOCIATED CONTENT

Supporting Information

The Supporting Information is available free of charge at https://pubs.acs.org/doi/10.1021/jasms.3c00453.

Amino acid sequences for all protein constructs, figures for monoisotopic masses, binding curve analyses, molecular dynamics simulations, dimer abundance, complementary collision-induced dissociation experiments for SFG, Cap-0 RNA binding, and retention, and Cap-1 RNA reaction progress (PDF)

■ AUTHOR INFORMATION

Corresponding Author

Mowei Zhou − *Environmental Molecular Sciences Laboratory, Pacific Northwest National Laboratory, Richland, Washington 99354, United States;* Present Address: Department of Chemistry, Zhejiang University, Hangzhou, Zhejiang 310058, China; orcid.org/0000-0003-3575-3224; Email: moweizhou@zju.edu.cn

Authors

Stephanie M. Thibert − *Environmental Molecular Sciences Laboratory, Pacific Northwest National Laboratory, Richland, Washington 99354, United States*

Deseree J. Reid − *Chemical and Biological Signature Sciences, Pacific Northwest National Laboratory, Richland, Washington 99354, United States*

Jesse W. Wilson − *Environmental Molecular Sciences Laboratory, Pacific Northwest National Laboratory, Richland, Washington 99354, United States;* orcid.org/0000-0002-2304-2540

Rohith Varikoti − *Biological Sciences Division, Pacific Northwest National Laboratory, Richland, Washington 99354, United States*

Natalia Maltseva − *Center for Structural Biology of Infectious Diseases, Consortium for Advanced Science and Engineering, University of Chicago, Chicago, Illinois 60637, United States; Structural Biology Center, X-ray Science Division, Argonne National Laboratory, Argonne, Illinois 60439, United States*

Katherine J. Schultz − *Biological Sciences Division, Pacific Northwest National Laboratory, Richland, Washington 99354, United States*

Agustin Kruel − *Biological Sciences Division, Pacific Northwest National Laboratory, Richland, Washington 99354, United States;* orcid.org/0000-0002-5571-7418

Gyorgy Babnigg − *Center for Structural Biology of Infectious Diseases, Consortium for Advanced Science and Engineering, University of Chicago, Chicago, Illinois 60637, United States; Biosciences Division, Argonne National Laboratory, Argonne, Illinois 60439, United States;* orcid.org/0000-0002-9838-1803

Andrzej Joachimiak − *Center for Structural Biology of Infectious Diseases, Consortium for Advanced Science and Engineering, University of Chicago, Chicago, Illinois 60637, United States; Structural Biology Center, X-ray Science Division, Argonne National Laboratory, Argonne, Illinois 60439, United States*

Neeraj Kumar − *Biological Sciences Division, Pacific Northwest National Laboratory, Richland, Washington 99354, United States;* orcid.org/0000-0001-6713-2129

Complete contact information is available at: https://pubs.acs.org/10.1021/jasms.3c00453

Author Contributions

SMT: Formal analysis, Data Curation, Writing − Original Draft, Writing − Review & Editing. **DJR:** Formal analysis, Data Curation, Writing − Original Draft, Writing − Review & Editing. **JWW:** Formal analysis, Investigation. **RV:** Formal analysis, Investigation, Writing − Review & Editing. **NM:** Resource, Writing − Review & Editing. **KJS:** Investigation, Resource, Writing − Review & Editing. **AK:** Investigation, Resource. **GB:** Resource, Writing − Review & Editing. **AJ:** Resource, Writing − Review & Editing, Funding acquisition. **NK:** Conceptualization, Writing − Review & Editing, Funding acquisition. **MZ:** Conceptualization, Formal analysis, Data Curation, Writing − Original Draft, Writing − Review & Editing, Project administration, Funding acquisition.

Author Contributions

†S.T.M., D.J.R., and J.W.W. contributed equally.

Notes

The authors declare no competing financial interest.

■ ACKNOWLEDGMENTS

We thank Ryan Choi and Wesley Van Voorhis at University of Washington for providing the alternative nsp10 construct, supported by the Seattle Structural Genomics Center for Infectious Diseases under Contract No. HHSN272201700059C. We also thank Dalton Snyder, Benjamin Jones, and Vicki Wysocki for providing the SID device under funding by the NIH National Institute of General Sciences using grant P41GM128577 (Wysocki). This research was supported by the EBSD Mission Seed, under the Laboratory Directed Research and Development (LDRD) Program at Pacific Northwest National Laboratory (PNNL), performed at the Environmental Molecular Sciences Laboratory (EMSL) under project 60268 (doi.org/10.46936/staf.proj.2021.60268/60008436) and in part by the National Institute of Allergy and Infectious Diseases, National Institutes of Health, Department of Health and Human Services, under Contract 75N93022C00035 (AJ) and by the DOE Office of Science through the National Virtual Biotechnology Laboratory, a consortium of DOE national laboratories focused on response to COVID-19, with funding provided by the Coronavirus CARES Act (AJ). PNNL is a multiprogram national laboratory operated for the U.S. Department of Energy (DOE) by Battelle Memorial Institute under Contract No. DE-AC05-76RL01830.

■ REFERENCES

(1) Batool, M.; Ahmad, B.; Choi, S. A Structure-Based Drug Discovery Paradigm. *International Journal of Molecular Sciences* **2019**, *20* (11), 2783.

(2) Yang, X.; Wang, Y.; Byrne, R.; Schneider, G.; Yang, S. Concepts of Artificial Intelligence for Computer-Assisted Drug Discovery. *Chem. Rev.* **2019**, *119* (18), 10520−10594.
(3) Joshi, R. P.; Kumar, N. Artificial Intelligence for Autonomous Molecular Design: A Perspective. *Molecules* **2021**, *26*, 6761.
(4) Joshi, R. P.; Schultz, K. J.; Wilson, J. W.; Kruel, A.; Varikoti, R. A.; Kombala, C. J.; Kneller, D. W.; Galanie, S.; Phillips, G.; Zhang, Q.; et al. AI-Accelerated Design of Targeted Covalent Inhibitors for SARS-CoV-2. *J. Chem. Inf. Model.* **2023**, *63* (5), 1438−1453.
(5) Varikoti, R. A.; Schultz, K. J.; Kombala, C. J.; Kruel, A.; Brandvold, K. R.; Zhou, M.; Kumar, N. Integrated data-driven and experimental approaches to accelerate lead optimization targeting SARS-CoV-2 main protease. *Journal of Computer-Aided Molecular Design* **2023**, *37* (8), 339−355.
(6) Zhou, M.; Lantz, C.; Brown, K. A.; Ge, Y.; Pasa-Tolic, L.; Loo, J. A.; Lermyte, F. Higher-order structural characterisation of native proteins and complexes by top-down mass spectrometry. *Chem. Sci.* **2020**, *11* (48), 12918−12936.
(7) Gavriilidou, A. F. M.; Sokratous, K.; Yen, H. Y.; De Colibus, L. High-Throughput Native Mass Spectrometry Screening in Drug Discovery. *Front Mol. Biosci* **2022**, *9*, 837901.
(8) Gu, Y.; Liu, M.; Quinn, R. J. Metabolite-protein interactions: Native mass spectrometry and collision induced affinity selection mass spectrometry in natural product screening. *Frontiers in Analytical Science* **2022**, DOI: 10.3389/frans.2022.1014017.
(9) Pukala, T.; Robinson, C. V. Introduction: Mass Spectrometry Applications in Structural Biology. *Chem. Rev.* **2022**, *122* (8), 7267−7268.
(10) VanAernum, Z. L.; Busch, F.; Jones, B. J.; Jia, M.; Chen, Z.; Boyken, S. E.; Sahasrabuddhe, A.; Baker, D.; Wysocki, V. H. Rapid online buffer exchange for screening of proteins, protein complexes and cell lysates by native mass spectrometry. *Nat. Protoc.* **2020**, *15* (3), 1132−1157.
(11) Thibert, S. M.; Bracken, C. C.; Orton, D. J.; Gibbons, B. C.; Zhou, M. A Simple and Flexible Infusion Platform for Automated Native Mass Spectrometry Analysis. *J. Am. Soc. Mass Spectrom.* **2023**, *34* (7), 1528−1531.
(12) Gavriilidou, A. F. M.; Sokratous, K.; Yen, H.-Y.; De Colibus, L. High-Throughput Native Mass Spectrometry Screening in Drug Discovery. *Frontiers in Molecular Biosciences* **2022**, DOI: 10.3389/fmolb.2022.837901.
(13) Park, H. M.; Winton, V. J.; Drader, J. J.; Manalili Wheeler, S.; Lazar, G. A.; Kelleher, N. L.; Liu, Y.; Tran, J. C.; Compton, P. D. Novel Interface for High-Throughput Analysis of Biotherapeutics by Electrospray Mass Spectrometry. *Anal. Chem.* **2020**, *92* (2), 2186−2193.
(14) Tamara, S.; den Boer, M. A.; Heck, A. J. R. High-Resolution Native Mass Spectrometry. *Chem. Rev.* **2022**, *122* (8), 7269−7326.
(15) Bennett, J. L.; Nguyen, G. T. H.; Donald, W. A. Protein-Small Molecule Interactions in Native Mass Spectrometry. *Chem. Rev.* **2022**, *122*, 7327.
(16) Zhou, M.; Lantz, C.; Brown, K. A.; Ge, Y.; Paša-Tolić, L.; Loo, J. A.; Lermyte, F. Higher-order structural characterisation of native proteins and complexes by top-down mass spectrometry. *Chemical Science* **2020**, *11* (48), 12918−12936.
(17) Versluis, C.; Heck, A. J. R. Gas-phase dissociation of hemoglobin. *Int. J. Mass Spectrom.* **2001**, *210*−*211*, 637−649.
(18) Sobott, F.; Hernández, H.; McCammon, M. G.; Tito, M. A.; Robinson, C. V. A tandem mass spectrometer for improved transmission and analysis of large macromolecular assemblies. *Anal. Chem.* **2002**, *74* (6), 1402−1407.
(19) Zhang, Y.; Deng, L.; Kitova, E. N.; Klassen, J. S. Dissociation of Multisubunit Protein-Ligand Complexes in the Gas Phase. Evidence for Ligand Migration. *Journal of The American Society for Mass Spectrometry* **2013**, *24* (10), 1573−1583.
(20) Zhou, M.; Yan, J.; Romano, C. A.; Tebo, B. M.; Wysocki, V. H.; Paša-Tolić, L. Surface Induced Dissociation Coupled with High Resolution Mass Spectrometry Unveils Heterogeneity of a 211 kDa Multicopper Oxidase Protein Complex. *J. Am. Soc. Mass Spectrom.* **2018**, *29* (4), 723−733.
(21) Busch, F.; VanAernum, Z. L.; Ju, Y.; Yan, J.; Gilbert, J. D.; Quintyn, R. S.; Bern, M.; Wysocki, V. H. Localization of Protein Complex Bound Ligands by Surface-Induced Dissociation High-Resolution Mass Spectrometry. *Anal. Chem.* **2018**, *90* (21), 12796−12801.
(22) VanAernum, Z. L.; Gilbert, J. D.; Belov, M. E.; Makarov, A. A.; Horning, S. R.; Wysocki, V. H. Surface-Induced Dissociation of Noncovalent Protein Complexes in an Extended Mass Range Orbitrap Mass Spectrometer. *Anal. Chem.* **2019**, *91* (5), 3611−3618.
(23) Malone, B.; Chen, J.; Wang, Q.; Llewellyn, E.; Choi, Y. J.; Olinares, P. D. B.; Cao, X.; Hernandez, C.; Eng, E. T.; Chait, B. T.; Shaw, D. E.; Landick, R.; Darst, S. A.; Campbell, E. A.; et al. Structural basis for backtracking by the SARS-CoV-2 replication-transcription complex. *Proc. Natl. Acad. Sci. U. S. A.* **2021**, *118* (19), No. e2102516118.
(24) Wilamowski, M.; Sherrell, D. A.; Minasov, G.; Kim, Y.; Shuvalova, L.; Lavens, A.; Chard, R.; Maltseva, N.; Jedrzejczak, R.; Rosas-Lemus, M.; et al. 2′-O methylation of RNA cap in SARS-CoV-2 captured by serial crystallography. *Proc. Natl. Acad. Sci. U. S. A.* **2021**, *118* (21), No. e2100170118.
(25) Benoni, R.; Krafcikova, P.; Baranowski, M. R.; Kowalska, J.; Boura, E.; Cahová, H. Substrate specificity of sars-cov-2 nsp10-nsp16 methyltransferase. *Viruses* **2021**, *13* (9), 1722.
(26) Krafcikova, P.; Silhan, J.; Nencka, R.; Boura, E. Structural analysis of the SARS-CoV-2 methyltransferase complex involved in RNA cap creation bound to sinefungin. *Nat. Commun.* **2020**, *11* (1), 3717−3717.
(27) Decroly, E.; Debarnot, C.; Ferron, F.; Bouvet, M.; Coutard, B.; Imbert, I.; Gluais, L.; Papageorgiou, N.; Sharff, A.; Bricogne, G.; et al. Crystal Structure and Functional Analysis of the SARS-Coronavirus RNA Cap 2′-O-Methyltransferase nsp10/nsp16 Complex. *PLOS Pathogens* **2011**, *7* (5), No. e1002059.
(28) Chen, Y.; Su, C.; Ke, M.; Jin, X.; Xu, L.; Zhang, Z.; Wu, A.; Sun, Y.; Yang, Z.; Tien, P.; et al. Biochemical and Structural Insights into the Mechanisms of SARS Coronavirus RNA Ribose 2′-O-Methylation by nsp16/nsp10 Protein Complex. *PLOS Pathogens* **2011**, *7* (10), No. e1002294.
(29) Vithani, N.; Ward, M. D.; Zimmerman, M. I.; Novak, B.; Borowsky, J. H.; Singh, S.; Bowman, G. R. SARS-CoV-2 Nsp16 activation mechanism and a cryptic pocket with pan-coronavirus antiviral potential. *Biophys. J.* **2021**, *120* (14), 2880−2889.
(30) Aouadi, W.; Blanjoie, A.; Vasseur, J. J.; Debart, F.; Canard, B.; Decroly, E. Binding of the Methyl Donor S-Adenosyl-l-Methionine to Middle East Respiratory Syndrome Coronavirus 2′-O-Methyltransferase nsp16 Promotes Recruitment of the Allosteric Activator nsp10. *J. Virol* **2017**, *91* (5), No. e02217-16.
(31) Bouvet, M.; Debarnot, C.; Imbert, I.; Selisko, B.; Snijder, E. J.; Canard, B.; Decroly, E. In Vitro Reconstitution of SARS-Coronavirus mRNA Cap Methylation. *PLOS Pathogens* **2010**, *6* (4), No. e1000863.
(32) Yan, W.; Zheng, Y.; Zeng, X.; He, B.; Cheng, W. Structural biology of SARS-CoV-2: open the door for novel therapies. *Signal Transduction and Targeted Therapy* **2022**, *7* (1), 26.
(33) Choi, R.; Zhou, M.; Shek, R.; Wilson, J. W.; Tillery, L.; Craig, J. K.; Salukhe, I. A.; Hickson, S. E.; Kumar, N.; James, R. M.; et al. High-throughput screening of the ReFRAME, Pandemic Box, and COVID Box drug repurposing libraries against SARS-CoV-2 nsp15 endoribonuclease to identify small-molecule inhibitors of viral activity. *PLoS One* **2021**, *16* (4), No. e0250019.
(34) Inniss, N. L.; Kozic, J.; Li, F.; Rosas-Lemus, M.; Minasov, G.; Rybáček, J.; Zhu, Y.; Pohl, R.; Shuvalova, L.; Rulíšek, L.; et al. Discovery of a Druggable, Cryptic Pocket in SARS-CoV-2 nsp16 Using Allosteric Inhibitors. *ACS Infectious Diseases* **2023**, *9*, 1918.
(35) Kim, Y.; Jedrzejczak, R.; Maltseva, N. I.; Wilamowski, M.; Endres, M.; Godzik, A.; Michalska, K.; Joachimiak, A. Crystal structure of Nsp15 endoribonuclease NendoU from SARS-CoV-2. *Protein Sci.* **2020**, *29* (7), 1596−1605.

(36) Makowska-Grzyska, M.; Kim, Y.; Maltseva, N.; Li, H.; Zhou, M.; Joachimiak, G.; Babnigg, G.; Joachimiak, A. Protein Production for Structural Genomics Using E. coli Expression. In *Structural Genomics and Drug Discovery: Methods and Protocols*; Anderson, W. F., Ed.; Springer: New York, 2014; pp 89−105.
(37) Snyder, D. T.; Panczyk, E. M.; Somogyi, A.; Kaplan, D. A.; Wysocki, V. Simple and minimally invasive SID devices for native mass spectrometry. *Anal. Chem.* **2020**, *92* (16), 11195−11203.
(38) Marty, M. T.; Baldwin, A. J.; Marklund, E. G.; Hochberg, G. K. A.; Benesch, J. L. P.; Robinson, C. V. Bayesian deconvolution of mass and ion mobility spectra: From binary interactions to polydisperse ensembles. *Anal. Chem.* **2015**, *87* (8), 4370−4376.
(39) Reid, D. J.; Diesing, J. M.; Miller, M. A.; Perry, S. M.; Wales, J. A.; Montfort, W. R.; Marty, M. T. MetaUniDec: High-Throughput Deconvolution of Native Mass Spectra. *J. Am. Soc. Mass Spectrom.* **2019**, *30* (1), 118−127.
(40) Abraham, M. J.; Murtola, T.; Schulz, R.; Páll, S.; Smith, J. C.; Hess, B.; Lindahl, E. GROMACS: High performance molecular simulations through multi-level parallelism from laptops to supercomputers. *SoftwareX* **2015**, *1−2*, 19−25.
(41) Maier, J. A.; Martinez, C.; Kasavajhala, K.; Wickstrom, L.; Hauser, K. E.; Simmerling, C. ff14SB: Improving the Accuracy of Protein Side Chain and Backbone Parameters from ff99SB. *J. Chem. Theory Comput.* **2015**, *11* (8), 3696−3713.
(42) Jorgensen, W. L.; Chandrasekhar, J.; Madura, J. D.; Impey, R. W.; Klein, M. L. Comparison of simple potential functions for simulating liquid water. *J. Chem. Phys.* **1983**, *79* (2), 926−935.
(43) Joung, I. S.; Cheatham, T. E., III. Determination of Alkali and Halide Monovalent Ion Parameters for Use in Explicitly Solvated Biomolecular Simulations. *J. Phys. Chem. B* **2008**, *112* (30), 9020−9041.
(44) Berendsen, H. J. C.; Postma, J. P. M.; van Gunsteren, W. F.; DiNola, A.; Haak, J. R. Molecular dynamics with coupling to an external bath. *J. Chem. Phys.* **1984**, *81* (8), 3684−3690.
(45) Parrinello, M.; Rahman, A. Polymorphic transitions in single crystals: A new molecular dynamics method. *J. Appl. Phys.* **1981**, *52* (12), 7182−7190.
(46) Darden, T.; York, D.; Pedersen, L. Particle mesh Ewald: An N·log(N) method for Ewald sums in large systems. *J. Chem. Phys.* **1993**, *98* (12), 10089−10092.
(47) Viswanathan, T.; Misra, A.; Chan, S.-H.; Qi, S.; Dai, N.; Arya, S.; Martinez-Sobrido, L.; Gupta, Y. K. A metal ion orients SARS-CoV-2 mRNA to ensure accurate 2′-O methylation of its first nucleotide. *Nat. Commun.* **2021**, *12* (1), 3287.
(48) Viswanathan, T.; Arya, S.; Chan, S.-H.; Qi, S.; Dai, N.; Misra, A.; Park, J.-G.; Oladunni, F.; Kovalskyy, D.; Hromas, R. A.; et al. Structural basis of RNA cap modification by SARS-CoV-2. *Nat. Commun.* **2020**, *11* (1), 3718.
(49) Hopper, J. T. S.; Robinson, C. V. Mass Spectrometry Quantifies Protein Interactions—From Molecular Chaperones to Membrane Porins. *Angew. Chem., Int. Ed.* **2014**, *53* (51), 14002−14015.
(50) Bui, D. T.; Li, Z.; Kitov, P. I.; Han, L.; Kitova, E. N.; Fortier, M.; Fuselier, C.; Granger Joly de Boissel, P.; Chatenet, D.; Doucet, N.; et al. Quantifying Biomolecular Interactions Using Slow Mixing Mode (SLOMO) Nanoflow ESI-MS. *ACS Central Science* **2022**, *8*, 963.
(51) Rogstam, A.; Nyblom, M.; Christensen, S.; Sele, C.; Talibov, V. O.; Lindvall, T.; Rasmussen, A. A.; André, I.; Fisher, Z.; Knecht, W.; et al. Crystal Structure of Non-Structural Protein 10 from Severe Acute Respiratory Syndrome Coronavirus-2. *International Journal of Molecular Sciences* **2020**, *21* (19), 7375.
(52) Lin, S.; Chen, H.; Ye, F.; Chen, Z.; Yang, F.; Zheng, Y.; Cao, Y.; Qiao, J.; Yang, S.; Lu, G. Crystal structure of SARS-CoV-2 nsp10/nsp16 2′-O-methylase and its implication on antiviral drug design. *Signal Transduction and Targeted Therapy* **2020**, *5* (1), 131.
(53) Lermyte, F.; Tsybin, Y. O.; O'Connor, P. B.; Loo, J. A. Top or Middle? Up or Down? Toward a Standard Lexicon for Protein Top-Down and Allied Mass Spectrometry Approaches. *J. Am. Soc. Mass Spectrom.* **2019**, *30* (7), 1149−1157.
(54) Zhou, M.; Dagan, S.; Wysocki, V. H. Protein subunits released by surface collisions of noncovalent complexes: nativelike compact structures revealed by ion mobility mass spectrometry. *Angew. Chem., Int. Ed. Engl.* **2012**, *51* (18), 4336−4339.
(55) Stiving, A. Q.; VanAernum, Z. L.; Busch, F.; Harvey, S. R.; Sarni, S. H.; Wysocki, V. H. Surface-Induced Dissociation: An Effective Method for Characterization of Protein Quaternary Structure. *Anal. Chem.* **2019**, *91* (1), 190−209.
(56) Zhou, M.; Dagan, S.; Wysocki, V. H. Impact of charge state on gas-phase behaviors of noncovalent protein complexes in collision induced dissociation and surface induced dissociation. *Analyst* **2013**, *138* (5), 1353−1353.
(57) Hall, Z.; Politis, A.; Bush, M. F.; Smith, L. J.; Robinson, C. V. Charge-State Dependent Compaction and Dissociation of Protein Complexes: Insights from Ion Mobility and Molecular Dynamics. *J. Am. Chem. Soc.* **2012**, *134* (7), 3429−3438.
(58) Snyder, D. T.; Harvey, S. R.; Wysocki, V. H. Surface-induced Dissociation Mass Spectrometry as a Structural Biology Tool. *Chem. Rev.* **2022**, *122* (8), 7442−7487.
(59) Konermann, L.; Aliyari, E.; Lee, J. H. Mobile Protons Limit the Stability of Salt Bridges in the Gas Phase: Implications for the Structures of Electrosprayed Protein Ions. *J. Phys. Chem. B* **2021**, *125*, 3803.
(60) Thachuk, M.; Fegan, S. K.; Raheem, N. Description and control of dissociation channels in gas-phase protein complexes. *J. Chem. Phys.* **2016**, *145* (6), 065101−065101.
(61) Loo, R. R. O.; Loo, J. A. Salt Bridge Rearrangement (SaBRe) Explains the Dissociation Behavior of Noncovalent Complexes. *J. Am. Soc. Mass Spectrom.* **2016**, *27* (6), 975−990.

https://doi.org/10.1021/jasms.3c00453
J. Am. Soc. Mass Spectrom. 2024, 35, 912−921